

Probing Topological Electronic Effects in Catalysis: Thiophene Adsorption on NiMoS and CoMoS Clusters

Itamar Borges Jr.^{*,a,b} and *Alexander M. Silva*^b

*^aDepartamento de Química and ^bPrograma de Pós-Graduação em Engenharia de Defesa,
Instituto Militar de Engenharia, Praça General Tibúrcio, 80, Praia Vermelha,
Rio de Janeiro-RJ 22290-270, Brazil*

Um método teórico geral em duas etapas para estudar redistribuições eletrônicas em processos catalíticos é apresentado. Na primeira etapa, teoria do funcional da densidade (DFT) é usada para otimizar completamente duas geometrias: o aglomerado que representa o catalisador e o sistema aglomerado mais molécula adsorvida. Na segunda etapa, a densidade eletrônica molecular convergida é dividida em multipolos centrados em sítios atômicos obtidos segundo uma análise de multipolos distribuídos, que fornece informação topológica detalhada da redistribuição de carga do catalisador e da molécula, antes e depois da adsorção. Esta abordagem é aplicada para a adsorção de tiofeno sobre a borda metálica 1010 dos catalisadores Ni(Co)MoS e comparada com a mesma reação em MoS₂ não-substituído. Energias de adsorção, geometrias e a análise de multipolos calculada indicam uma fraca adsorção do tiofeno em ambas as situações. Um modelo coulombiano para a ligação química mostra que a magnitude da ligação metal-enxofre na superfície dos catalisadores de Ni(Co)MoS promovidos é consideravelmente menor do que em MoS₂ não substituído, desta forma confirmando a origem do aumento da atividade de hidrodesulfurização (HDS) nestes catalisadores.

A general two-step theoretical approach to study electronic redistributions in catalytic processes is presented. In the first step, density functional theory (DFT) is used to fully optimize two geometries: the cluster representing the catalyst and the cluster plus adsorbed molecule system. In the second step, the converged electron density is divided into multipoles centered on atomic sites according to a distributed multipole analysis which provides detailed topological information on the charge redistribution of catalyst and molecule before and after adsorption. This approach is applied to thiophene adsorption on the 1010 metal edge of Ni(Co)MoS catalysts and compared to the same reaction on bare MoS₂. Calculated adsorption energies, geometries and multipole analysis indicate weak thiophene chemisorption on both cases. A Coulombic bond model showed that surface metal-sulfur bond strengths in Ni(Co)MoS promoted catalysts are considerably smaller than in bare MoS₂, thus confirming the origin of the enhancement of hydrodesulfurization (HDS) activity in these catalysts.

Keywords: charge redistribution, hydrodesulfurization (HDS), promoter effect

Introduction

Theoretical investigation of molecular processes is usually based on the concept of molecular orbitals (MOs). In most cases, self-consistent, or Hartree-Fock (HF) orbitals, is used. On the other hand, the use of density functional theory (DFT) molecular orbitals is prone to criticism since the Kohn-Sham orbitals, being only a basis set to expand the electron density, lack physical sense. However,

although the use of self-consistent MOs definitely enriches interpretation of chemical phenomena, it would be interesting to have a distinct and original perspective. In this work, a physically and chemically motivated method is employed to partition an optimized molecular electron density which, in contrast to self-consistent MOs, includes electron correlation. By investigating the first step in an important hydrotreatment catalytic process, the wealth of detailed information that can be obtained from this general approach is shown.

In hydrotreatment processes such as hydrodesulfurization (HDS), hydrogenation (HYD) and hydrodenitrogenation

*e-mail: itamar@ime.eb.br

(HDN), promoted catalysts based on molybdenum sulfides are widely used. The most employed HDS catalysts consist of a mixture of Ni or Co with MoS₂.¹⁻³ These mixtures show high HDS activity, whereas mixing other transition metals with MoS₂ shows only a weak or moderate promotional effect.⁴ From a fundamental point of view, the structure and function of the active sites, the role of the promoter in the reaction and the hydrogen-activation mechanism, despite recent theoretical and experimental advances, can benefit from new insights.^{5,6} The adsorption geometry and bonding mode of organic molecules on the MoS₂-catalyst edge surfaces are also not totally understood.⁷ Therefore, new theoretical work can lead to increased understanding of the relationships between activity and structure of hydrotreatment catalysis, especially at the atomic level.

The MoS₂ catalysts, in addition to their importance for HDS processes, have applications as single-layered MoS₂ nanotubes, effective solid lubricants,⁸ among others.⁹

A considerable number of experimental and theoretical studies have been devoted to elucidate active sites of bare MoS₂ catalysts and to investigate the associated HDS mechanism. In particular, thiophene adsorbed on bare MoS₂ is one of the most studied theoretical catalyst models. As a prototype system, thiophene adsorption on MoS₂ catalysts has been theoretically investigated using the two available approaches to describe a catalyst in the DFT framework: cluster models of different sizes¹⁰⁻¹⁴ and periodic boundary conditions.^{15,16}

Concerning promoted systems, there are some theoretical works on surface properties and adsorption of molecules on Ni(Co)MoS catalysts using DFT with periodic boundary conditions¹⁷⁻²¹ and cluster models.^{5,22} There are recent reviews on the subject.^{7,23,24} Results from scanning-tunneling-microscopy (STM) experiments^{25,26} and systematic DFT calculations^{24,27} suggest the decoration or Co–Mo–S model as the most probable model of substituted MoS₂ catalysts. In this model, Co or Ni promoter atoms substitute Mo atoms in the edge planes.

For thiophene and other sulfur molecules adsorbed on Co- and Ni-promoted MoS₂ catalysts, quantum-mechanical calculations are rather scarce, in contrast to adsorption on bare MoS₂ catalysts. Sun *et al.*²⁸ calculated, with DFT and periodic boundary conditions, adsorption thermodynamic data of several important molecules, including thiophene, for NiMoS hydrotreatment processes. Weber and van Veen²⁹ used DFT to investigate HDS of dibenzothiophene on a NiMoS cluster including one Ni atom and 18 Mo atoms.

There are few DFT works using topological approaches bearing some similarity to our work, but using different methods. Krebs *et al.*²² studied the adsorption modes

of toluene and 2-methylthiophene on Ni(Co)MoS₂ catalyst and did a topological analysis using electron localization functions (ELF). Joshi *et al.*³⁰ used natural bond orbital (NBO)-based electronic descriptors to describe the adsorption energy variation for 12 sulfur-containing molecules. Aray and Rodríguez³¹ employed DFT and periodic boundary conditions to study the nature of MoS₂ edges related to the creation of sulfur vacancies. The same group studied NiMoS using the same approach and electrostatic potential mapping, showing that the main role of the promoter is to produce sulfur-uncovered Lewis acids.³² In a preliminary work on the method proposed here, our group studied thiophene molecule adsorption on the 10 $\bar{1}0$ plane (Mo edge) of a Mo₁₆S₃₂ cluster applying the distributed multipole analysis (DMA) decomposition.³³ Recently, also using the DMA method, our group examined MoS₂ model clusters of different sizes and concluded that a Mo₁₆S₃₂ cluster can adequately represent the electronic structure of real size MoS₂ edges.³⁴

The purpose of this work is to present a general approach to investigate topological properties of surfaces and reactions. The method is applied to Ni(Co)MoS HDS-promoted catalysts and adsorption of thiophene on their metal edges. A detailed topological picture of the surfaces before and after adsorption is presented. It is also discussed the origin of the promoter effect on both surfaces.

Methodology

Computational approach

DFT methods were used in this work. However, the method employed to divide the electron density is independent of the electronic structure approach. Wave function methods such as MP2 can be employed as well.

Calculations were done using the B3LYP functional,³⁵ the LACVP** basis set (6–31G** and effective core potentials for Ni and Co)³⁶ and the Gaussian 03 program.³⁷ To improve DFT convergence, the G03 default parameters and quadratic convergence (QC) methods were used, the latter recommended for transition metal systems. The Jaguar program³⁸ was used with the same method for preliminary convergence tests of the cluster geometries and thiophene desorption. The Jaguar default convergence parameters were employed.

The B3LYP functional was used because thiophene adsorption on bare MoS₂ was previously studied with the same method³³ and to allow comparisons with the present results. However, it is important to take under consideration that dispersion interactions, which can play an important role in adsorption processes, are not well described with B3LYP.³⁹

Based on the decoration model, the three Mo edge atoms in the $10\bar{1}0$ planes were substituted by Co promoter atoms in the CoMoS cluster and by Ni promoter atoms in NiMoS. In this way, the present results can be compared directly with previous results of thiophene adsorption on a bare MoS_2 edge of same size.³³ Geometry-optimization calculations were carried out to obtain minimum structures of the $\text{Ni}_3\text{Mo}_{13}\text{S}_{32}$ and $\text{Co}_3\text{Mo}_{13}\text{S}_{32}$ isolated clusters before (Figure 1) and after thiophene adsorption (Figure 2). Vibrational frequencies were calculated to check the nature of the stationary points and to discuss the adsorption process.

It should be noted that loading of promoter atoms (that is, the number of Ni and Co atoms substituting Mo atoms in the surface) is largely dependent on sulfidation conditions and can be smaller than full substitution.²⁰ However, to compare bare MoS_2 results³³ with the present ones and to investigate the promotion effect, we constructed the promoted clusters with this load. For the same reason, we used singlet multiplicity for the calculations.

From DFT calculations on MoS_2 clusters, Orita *et al.*⁴⁰ suggested that 16 metal and 32 sulfur atom cluster models would have the smallest acceptable cluster size for theoretical investigations; also previously shown by our group using the distributed multipole analysis (DMA).³⁴ DMA was computed from the DFT one-electron density matrix using the GDMA2 program of Stone.⁴¹

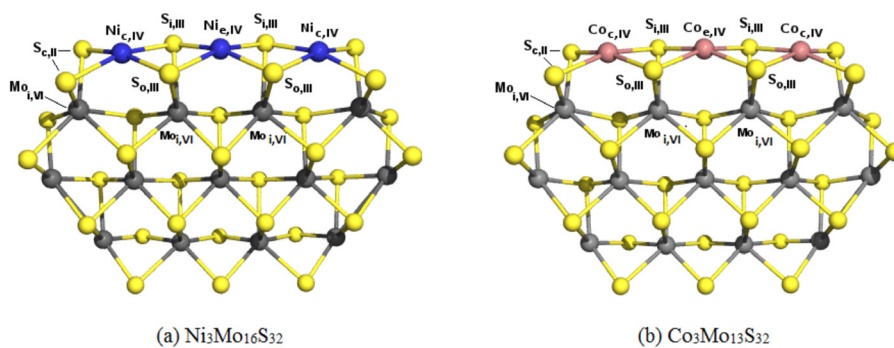


Figure 1. Optimized structures of (a) $\text{Ni}_3\text{Mo}_{16}\text{S}_{32}$ and (b) $\text{Co}_3\text{Mo}_{13}\text{S}_{32}$.

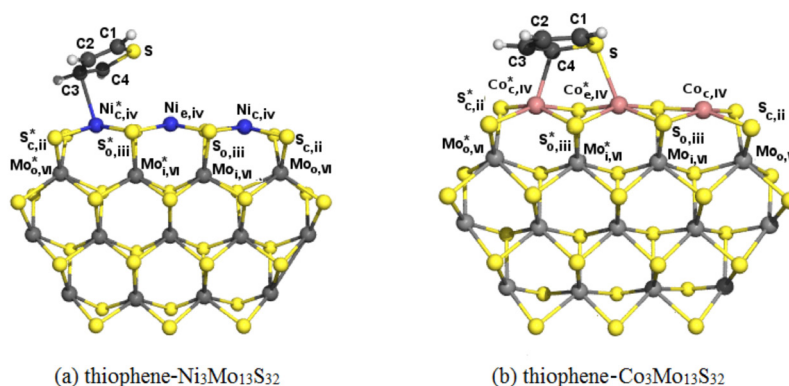


Figure 2. Optimized structures of (a) thiophene- $\text{Ni}_3\text{Mo}_{13}\text{S}_{32}$ and (b) thiophene- $\text{Co}_3\text{Mo}_{13}\text{S}_{32}$. The starred surface atoms are the closest to adsorbed thiophene.

Partition of the electron density

Electron density is a central property. From the fundamental theorem of DFT, the external potential is univocally determined by the electron density. As a corollary, the electron density ultimately determines the wave function.⁴² The electron density either measured or computed can be decomposed in several ways. In this work, it was explored one possibility.

In previous works, our group used the DMA method to study thiophene adsorption on MoS_2 ,³³ properties of molecules with potential to be new energetic materials⁴³ and relations between charge density and sensitivity properties in nitroaromatic molecules.⁴⁴ Recently, our group used another atom-centered partition scheme, the deformed atoms in molecules (DAM) model^{45,46} to partition electron density of four conformers of hexahydro-1,3,5-trinitro-1,3,5-triazine energetic molecule, known as RDX, and examined their electronic structure and fragmentation modes.⁴⁷

Partition of the molecular charge according to DMA was developed with the main purpose of evaluating intermolecular interactions, being also useful to investigate accurately molecular charge distributions.^{41,48-50} The method divides the molecular charge density into regions, each one described by its own electric multipole moments.

In this work, a region is an atomic site of the thiophene molecule and the Ni(Co)MoS clusters.

According to DMA, the electron density is divided into a sum of a product of atom-centered Gaussian basis functions, with coefficients determined from the one-electron density matrix. Any individual product of atom-centered basis functions is taken as a sum of multipole moments of ranks up to the degree of its polynomial. Therefore, the overlap of two s functions can be expressed as localized charge (monopole), the product of an s with a p function as a charge plus a dipole, the overlap of two p functions generates charge, dipole and quadrupole moments, and so on. If orbitals are on different atoms, then each pair of Gaussian functions produces a finite electric multipole series at a point between the two atoms determined by exponents of involved Gaussian orbitals. These multipoles are represented by a series on the nearest atom or another expansion site. DMA evaluates these exact representations and approximates each of them by a multipole expansion, usually on the atomic nuclei. This series rapidly converges due to expansion on different points of the electron charge distribution. By combining electron charge densities with nuclei positive charge values, the molecular charge density is obtained, as reported below.

The DMA expansion terms have a clear-cut interpretation. The monopole term corresponds to localized charges on atomic sites; bonds between adjacent atoms with different charge values indicate charge separations. Bond densities result in significant site dipole moments, which depend on the electronegativity of adjacent atoms and their molecular environment. Dipole moments reflect atomic polarization, generally followed by charge separation in the opposite direction.⁵¹ The quadrupole moment is the first electrostatic moment to include contributions from "out-of-plane density": it is related to delocalized electrons (π electrons) and may have contributions from lone-pair electrons.⁴⁹ Since DMA provides an accurate description of molecular charge densities, the method can be used to study intermolecular interactions and rationalize chemical bonding.^{33,43,52-54}

For dipole moments, a vector, it is reported their magnitudes and for quadrupole moments, a tensor, it is presented a number corresponding to the square-root of the sum of all tensor components squared.

The charge distribution of interacting molecules determines their intermolecular interactions,⁵³ thus knowing accurately this property allows one to investigate any molecular process in detail. The DMA decomposition, derived from an accurate computed electron density, gives this possibility. It should be noted that DMA is

considerably more accurate than methods providing site charges.

Results and Discussion

The geometry of Ni₃Mo₁₃S₃₂ and Co₃Mo₁₃S₃₂ clusters

The final Ni₃Mo₁₃S₃₂ and Co₃Mo₁₃S₃₂ optimized structures are displayed in Figure 1. The decorated metallic 10 $\bar{1}0$ edge of both clusters, with four-coordinated metal atoms, is quasi-planar, in agreement with previous works using DFT and periodic boundary conditions²⁴ and a cluster model of same size (but with only one promoted atom in the edge).⁵

The peripheral edges consist only of $\bar{1}010$ (S edge) and $10\bar{1}0$ planes (Ni and Co edges). The decorated edges in this work are only the $10\bar{1}0$ metal planes. Different S atoms in both clusters can be classified into two types^{5,55} according to their coordination number and charge properties; they are labelled S_{c,II} and S_{o,II}. The c and o subscripts represent corner and outer atomic positions, and the Roman numeral indicates the coordination number of each atom. Using a similar notation for Ni, Co and Mo, there are corner (c), edge (e) and inner (i) metal atoms (Figure 1). The promoter atoms (Ni_{c,IV}, Ni_{e,IV}, and Co_{c,IV}, Co_{e,IV}) are twofold coordinatively unsaturated (CUS) sites for HDS reactions.^{5,55}

The most relevant geometrical parameters of the Ni₃Mo₁₃S₃₂ and Co₃Mo₁₃S₃₂ clusters are shown in Table 1. These values are compared to experimental data^{56,57} and calculations of Raybaud *et al.*¹⁸ using DFT with periodic boundary conditions. The periodic approach does not show the distortion in the metallic edge present in the cluster model, namely, a slightly distorted local structure around the Ni_{c,IV} and Co_{c,IV} atoms (Table 1). Despite the distortion, distances between metal atoms are in good agreement for both theoretical approaches. The geometric parameters for isolated and adsorbed thiophene molecule on the Ni₃Mo₁₃S₃₂ and Co₃Mo₁₃S₃₂ clusters can be found in Table 2.

The extended X-ray absorption fine structure (EXAFS) Ni–Mo and Co–Mo distances^{56,57} are, respectively, 2.85 and 2.80 Å, and our Ni_{c,IV}–Mo_{i,VI} and Co_{e,IV}–Mo_{i,VI} computed distances are 2.76 and 2.79 Å, respectively, in good agreement with experimental data. The Ni_{c,IV}–Mo_{i,VI}, Co_{c,IV}–Mo_{i,VI}, Ni_{e,IV}–Mo_{i,VI} and Co_{e,IV}–Mo_{i,VI} distances also agree favorably with experiment.

Both Ni–S and Co–S distances are a bit larger than experimental values, and a slight distortion is also present. Overall, our values for both clusters agree with Raybaud *et al.*¹⁸ DFT values despite the slight distortion in the former, which does not have the intrinsic advantage of using periodic boundary conditions.

Table 1. Geometric parameters for the Ni₃Mo₁₃S₃₂ and Co₃Mo₁₃S₃₂ clusters

Parameter	Ni ₃ Mo ₁₃ S ₃₂	Co ₃ Mo ₁₃ S ₃₂	Experimental ^a	Calculated ^b
Distance / Å				
Ni _{c,IV} -Ni _{e,IV}	3.34	–	–	–
Ni _{c,IV} -Mo _{o,VI}	2.66	–	2.85	2.75
Ni _{c,IV} -Mo _{i,VI}	2.86	–	2.85	2.75
Ni _{e,IV} -Mo _{i,VI}	2.76	–	2.85	2.75
Ni _{e,IV} -Mo _{o,VI}	5.46	–	–	–
Ni _{c,IV} -S _{c,II}	2.30	–	–	2.17
Ni _{c,IV} -S _{o,III}	2.25	–	–	2.17
Ni _{e,IV} -S _{o,III}	2.25	–	–	2.17
Co _{e,IV} -Co _{e,IV}	–	3.38	–	–
Co _{c,IV} -Mo _{o,VI}	–	2.66	2.80	2.84
Co _{c,IV} -Mo _{i,VI}	–	2.72	2.80	2.84
Co _{e,IV} -Mo _{i,VI}	–	2.79	2.80	2.84
Co _{e,IV} -Mo _{o,VI}	–	5.51	–	–
Co _{c,IV} -S _{c,II}	–	2.27	2.18-2.24	2.21
Co _{c,IV} -S _{o,III}	–	2.27	2.18-2.24	2.21
Co _{e,IV} -S _{o,III}	–	2.31	2.18-2.24	2.21
Angle / degree				
S _{c,II} -Ni _{c,IV} -S _{c,II}	87.1	–	–	–
S _{o,III} -Ni _{c,IV} -S _{o,III}	82.5	–	–	–
S _{o,III} -Ni _{e,IV} -S _{o,III}	82.4	–	–	–
S _{c,II} -Co _{c,IV} -S _{c,II}	–	88.2	–	–
S _{o,III} -Co _{c,IV} -S _{o,III}	–	83.8	–	–
S _{o,III} -Co _{e,IV} -S _{o,III}	–	82.2	–	–

^aFrom references Bouwens *et al.*⁵⁶ and Leliveld *et al.*⁵⁷ ^bfrom Raybaud *et al.*¹⁸

Electronic structure of thiophene, Ni₃Mo₁₃S₃₂ and Co₃Mo₁₃S₃₂

The calculated charges (Q₀), dipole (Q₁) and quadrupole moments (Q₂) of atoms of the Ni₃Mo₁₃S₃₂, Co₃Mo₁₃S₃₂ and Mo₁₆S₃₂ clusters and isolated thiophene are shown in Tables S1-S4 in the Supplementary Information (SI) section. The labeling of atoms follows from Figures 1 and 2.

In thiophene (Table S4), carbon atoms bonded to sulfur have the largest negative charges, which are approximately five times larger when compared to the charge of the carbons bonded only to hydrogen. The sulfur atom has an appreciable positive charge, indicating a large S⁺C⁻ charge separation and a considerable dipole value (Q₁); the nearest carbon atoms are also well polarized. These two results combined reveal a quite general charge-separation bond polarization effect,⁵¹ thus providing a picture of chemical bond not present in other types of population analysis. The large values of the quadrupole moments in all atoms clearly reflect the well-known thiophenic π system.

The dipole values (Q₁) of atoms in the metallic edge of Ni₃Mo₁₃S₃₂ and Co₃Mo₁₃S₃₂ (Tables S1 and S2) are compared with those in bare MoS₂ of same size before thiophene adsorption (Table S3: previous results³³ shown in the same notation).

A dipole value of 0.30 *ea*₀ (= 0.76 D) is about 40% smaller in comparison to the value of a water molecule (= 0.7298 *ea*₀ = 1.855 D). In bare MoS₂, corner S atoms have about half the dipole values when compared to corner sulfur atoms in both promoted catalysts, a situation leading to lower interactions in bare MoS₂.

For corner metal atoms (Co_{c,IV} and Ni_{c,IV}), the dipole value of Co_{c,IV} is approximately 40% higher than in Ni_{c,IV} and 5 times higher than Mo_{c,IV} in bare MoS₂ (0.07 *ea*₀). The dipole value in the Co_{e,IV} edge atom is the largest, being twice the Ni_{e,IV} value and three times the Mo_{e,IV} value, and is similar to the corner cobalt atom (Co_{c,IV}) value. For sulfur atoms in NiMoS and CoMoS clusters, corner and outer sulfur dipoles have similar values of approximately 0.30 *ea*₀, the corner S atoms in pure MoS₂

Table 2. Geometric parameters for the isolated thiophene and thiophene adsorbed on $\text{Ni}_3\text{Mo}_{13}\text{S}_{32}$ and $\text{Co}_3\text{Mo}_{16}\text{S}_{32}$ clusters

Parameter	Isolated thiophene		Adsorbed thiophene	
	Experimental	Calculated	$\text{Ni}_3\text{Mo}_{16}\text{S}_{32}$	$\text{Co}_3\text{Mo}_{16}\text{S}_{32}$
Distance / Å				
S–C1	1.71	1.73	1.74	1.76
S–C4	1.71	1.73	1.72	1.79
C1–C2	1.37	1.37	1.36	1.35
C2–C3	1.42	1.43	1.44	1.45
C3–C4	1.37	1.37	1.39	1.39
S–Ni [*] _{e,IV}	–	–	3.64	–
C2–Ni [*] _{e,IV}	–	–	3.20	–
C3–Ni [*] _{e,IV}	–	–	2.43	–
C4–Ni [*] _{e,IV}	–	–	2.65	–
Ni [*] _{c,IV} –Ni _{e,IV}	–	–	3.36	–
Ni [*] _{c,IV} –Mo _{i,VI}	–	–	2.73	–
Ni [*] _{c,IV} –Mo _{i,VI}	–	–	2.88	–
Ni [*] _{c,IV} –S _{c,II}	–	–	2.30	–
Ni [*] _{c,IV} –S _{o,III}	–	–	2.28	–
Ni [*] _{c,IV} –S _{i,III}	–	–	2.27	–
S–Co _{e,IV}	–	–	–	2.51
C2–Co [*] _{e,IV}	–	–	–	3.25
C3–Co [*] _{e,IV}	–	–	–	2.39
C4–Co [*] _{e,IV}	–	–	–	2.22
Co [*] _{c,IV} –Co _{e,IV}	–	–	–	3.25
Co [*] _{c,IV} –Mo _{i,VI}	–	–	–	2.73
Co [*] _{c,IV} –Mo _{i,VI}	–	–	–	2.81
Co [*] _{c,IV} –S _{c,II}	–	–	–	2.27
Co [*] _{c,IV} –S _{o,III}	–	–	–	2.28
Co [*] _{c,IV} –S _{i,III}	–	–	–	2.28

bear a comparable value (0.29 ea_0) while the outer S atoms have about half of that value (0.16 ea_0).

In previous work,³³ our group verified that, after thiophene adsorption, site dipole moment values of S and Mo atoms in the Mo edge plane of bare MoS_2 increased substantially. In particular, in bare MoS_2 dipole moments of Mo surface atoms in the region over adsorbed thiophene increased by a factor of 10 and those of corner S atoms almost doubled. Moreover, dipole values of carbon atoms next to the sulfur atom of adsorbed thiophene increased by about 30%.

Considering thiophene adsorption on promoted catalysts, dipole values before and after adsorption in the sulfur sites do not show any appreciable variation (Tables S5 and S6 in the SI section), in contrast to thiophene adsorbed on bare MoS_2 . On the other hand, dipole values of Ni and Co atoms closer to adsorbed thiophene ($\text{Ni}_{c,IV}^*$, $\text{Ni}_{e,IV}^*$, $\text{Co}_{c,IV}^*$ and $\text{Co}_{e,IV}^*$) exhibit

considerable variation. For example, dipole value of corner Ni and edge Co atoms increased from 0.27 to 0.52 ea_0 and from 0.38 to 0.54 ea_0 , respectively. Concerning the adsorbed thiophene on both surfaces, there are not substantial changes in the dipole values of C atoms and only a small variation for the S atom. This small variation is more apparent in the thiophene plus $\text{Co}_3\text{Mo}_{16}\text{S}_{32}$ system, a pattern quite distinct when compared to thiophene adsorbed on bare MoS_2 .³³

According to the literature, the role of promoter atoms in improving the catalyst activity derives from reducing the average metal-sulfur (M–S) bond strength. The Co–S and Ni–S bonds, being weaker than a Mo–S bond, are broken more easily and result in increased number of vacancies in the edges.¹⁸ This behavior can be explained as follows.

From Tables S1 and S2, it can be seen that both corner and edge Ni and Co atoms have negative charges (Q_0), with values about 25% more negative in Ni-promoted cluster. On the other

hand, charges on Mo atoms in a bare MoS₂ cluster of same size (Table S3) are positive and more than three times the magnitude of metal atoms (Ni and Co) of promoted cluster. The negative charges in the Ni and Co atoms are followed, according to their Q₁ values, by considerable site polarization in comparison to bare MoS₂. All sulfur atoms in the three metal edges present negative charges, with the largest values being for S atoms in bare MoS₂ cluster.

In order to describe the nature of the bond strengths and provide quantitative information, a Coulombic bonding model can be used.^{58,59} In this way, consider that: (i) bond strengths are dominated by Coulombic interactions between DMA charges and thus are ion-ion like; (ii) only nearest-neighbor surface atoms contribute to the bond strength; (iii) distances between atoms are similar and; (iv) contributions from inner atoms to bond strengths are similar for the three clusters.

The promoter and sulfur atoms in both substituted clusters have negative charges. Note that charges are the localized part of decomposed charge densities, so there are also dipole and quadrupole moment contributions to fully describe the site density. Therefore, negative charges on the Ni and Co atom are possible in the DMA framework.

In contrast to promoted clusters, bare MoS₂ cluster has Mo atoms with positive charges and S atoms with negative charges; moreover, bare MoS₂ has the largest magnitude of charge values. Therefore, by substituting the computed DMA charges into the expression of the Coulombic interaction energy, it can be seen directly that ion-ion contribution to the bond strengths is positive in promoted clusters (i.e., repulsive for like-charges) and negative (i.e., attractive for opposite charges) in bare MoS₂. This situation clearly indicates decreased metal-sulfur bond strengths in promoted clusters in comparison to bare MoS₂, thus confirming theoretically the bond weakening as the origin of the promoter effect. Furthermore, since the magnitude of negative charges in the Ni and S atoms of Ni-promoted edge is larger than charges on Co and S atoms in the metal edge, NiMoS catalyst has the smallest bond strengths and thus produces vacancies more easily, thereby being the most effective catalyst, as actually happens.¹⁷ Naturally, this Coulombic model could be improved, in the context of DMA multipoles, by including ion-dipole, dipole-dipole and even higher multipole terms. However, these contributions would be considerably smaller,⁶⁰ very complicated to calculate and would not change the reasoning just given.

These results are in nice agreement with Allred and Rochow (A.E.) electronegativity scale, defined as the electrostatic force exerted by a nucleus on the valence electrons.⁶¹ In other words, the A.E. scale is the charge

experienced by an electron on the “surface” of an atom: the larger the charge *per* unit area of the atomic surface, the greater the tendency of that atom to attract electrons. Therefore, the A.E. scale is constructed according to similar ideas of the Coulombic model just discussed. So, not surprisingly, in the A.E. scale, the Mo atom is the less electronegative. Moreover, the A.E. electronegativity values are 1.30 for Mo, 1.7 for Co and 1.75 for Ni, with sulfur having a value of 2.44.

The interaction of adsorbed thiophene with promoted clusters is not as strong as with bare MoS₂, a picture which can be understood from the DMA. There are negative charges (Q₀) on Ni and Co surface atoms of promoted clusters and positive charges on Mo atoms of bare MoS₂. Additionally, quadrupole moments (Q₂) for Mo atoms in bare MoS₂ are considerably larger than in Ni and Co atoms of promoted catalysts. Thus, the Q₀ and Q₂ values favor thiophene-surface interaction in bare (non-promoted) MoS₂. In contrast, dipole (Q₁) values of corner Ni and Co atoms are about four times larger than in Mo atoms of bare MoS₂; for edge atoms, Q₁ values for Co are over three times and for Ni are 50% larger than in bare MoS₂. These dipole values indicate considerable site polarization of metal atoms in promoted catalysts in comparison to bare MoS₂. Therefore, a more localized bonding of adsorbed thiophene to surface atoms is favored in promoted clusters. Furthermore, our results show that thiophene-surface interaction in promoted catalysts is insufficient to destroy the molecular π system. In contrast, thiophene adsorbed on bare MoS₂ interacts with the surface through its π electron system, thereby leading to the non-localized η₃ bonding.³³

Inner and outer Mo atoms in the three clusters reveal in general similar multipoles values. The exception is the polarization (Q₁) of inner and outer Mo atoms in bare MoS₂, which is smaller than in promoted clusters, specially for Mo_{i,VI} (inner) atoms in the former. The quadrupole (Q₂) value in the Mo_{i,VI} site of bare MoS₂ is also much smaller. These multipole values show that these “missing” polarization and delocalized electrons in inner Mo (Mo_{i,VI}) probably contribute to greater electron density on the surface S atoms in bare MoS₂, in comparison to equivalent S atoms in promoted clusters.

Thiophene adsorption on the Ni₃Mo₁₃S₃₂ and Co₃Mo₁₃S₃₂ clusters

Experimental studies of desulfurization reactions on metal surfaces and with organometallic complexes⁶² show that the orientation of thiophene with respect to metal surfaces depends on the coverage of co-adsorbed hydrocarbons and sulfur atoms. On most surfaces, a parallel

geometry (η^5) is favored for low surface coverage while a more perpendicular ring orientation (η^1) is favored at high surface coverage. Quantum-mechanical calculations using DFT combined with cluster or periodic boundary condition models^{15,16,33,40} show that η^5 -type adsorption mode of thiophene is the most stable when a perfect metallic edge is considered. Therefore, we have limited ourselves only to starting configurations of thiophene parallel to the surface for geometry optimizations. However, we should bear in mind that, under catalytic conditions, the metallic edge is covered with bridged sulfur atoms³⁴ and the most favorable adsorption mode on this surface is a η^1 mode.¹⁶

The optimized configurations of adsorbed thiophene on the $\text{Ni}_3\text{Mo}_{13}\text{S}_{32}$ and $\text{Co}_3\text{Mo}_{13}\text{S}_{32}$ model catalysts are shown in Figure 2. The starred surface atoms are the closest to adsorbed thiophene molecule.

Thiophene adsorbs on the metallic edge of $\text{Ni}_3\text{Mo}_{13}\text{S}_{32}$ through two carbon atoms, C3 and C4 (Figure 2a), in a η^2 mode. The $\text{Ni}_{\text{c,IV}}^*-\text{C3}$ and $\text{Ni}_{\text{c,IV}}^*-\text{C4}$ bond distances are 2.43 and 2.65 Å, respectively. The planarity of the thiophene ring and thus, its π system, is preserved, in contrast to what happens for thiophene adsorption on the metallic edge of bare MoS_2 .^{15,33} Furthermore, the converged thiophene geometry after adsorption does present substantial changes. The surface multipole values of the Ni-promoted cluster discussed in the last section, which almost did not vary, confirm this trend; the same behavior also exists for thiophene adsorbed on Co-promoted cluster. This result is further corroborated from the small variations of thiophene multipoles before and after adsorption. The exception is the C3 atom, bonded to $\text{Ni}_{\text{c,IV}}^*$ and the thiophene atom closest to the surface: the charges (Q_0) almost double and the dipole (Q_1) increases by a factor over 5, an indication of combined charge separation and bond polarization of the C=C bond in thiophene. Thus, some bond weakening is induced by the surface through localized backdonation.

Regarding the Ni surface after thiophene adsorption, the prominent features are the polarization of $\text{Ni}_{\text{c,IV}}^*$ (Q_1 almost doubles) and an over 20% increase of its quadrupole (Q_2) value. Both results indicate a localized electron donation from the molecule to the surface. The quadrupole of $\text{Ni}_{\text{c,IV}}^*$ atom increases, while dipole and charge values do not change. These features reflect the presence of an interaction between delocalized NiMoS surface electrons and adsorbed thiophene. Concerning edge sulfur atoms, including those nearest to thiophene, the multipoles do not change significantly, a further indication of the preponderance of the role of edge metal atoms in thiophene-surface interaction.

When thiophene adsorption on the metallic edge of $\text{Co}_3\text{Mo}_{13}\text{S}_{32}$ is analyzed, some similarity with the adsorption on $\text{Ni}_3\text{Mo}_{13}\text{S}_{32}$ can be seen. Thiophene also adsorbs on the

$\text{Co}_3\text{Mo}_{13}\text{S}_{32}$ cluster through two carbon atoms, C3 and C4 but, unlike Ni catalyst, there is an evident S bonding to the surface. This bond type can be classified as $\eta^2-\text{C}$ and $\eta^1-\text{S}$. The $\text{Co}_{\text{c,IV}}-\text{C3}$, $\text{Co}_{\text{c,IV}}-\text{C4}$ and $\text{Co}_{\text{c,IV}}-\text{S}$ bond distances are 2.39, 2.22 and 2.51 Å, respectively (Table 2). The major changes of multipole values in thiophene before (Table S4) and after adsorption (Table S6) are as follows. The quadrupole values of C4 (changes from 1.68 to 1.27 ea^2_0) and C1 (from 1.68 to 1.47 ea^2_0) atoms decrease. For the S atom in thiophene, the charge increases (from 0.63 to 0.73 e) and the dipole and quadrupole decreases (from 1.19 to 0.91 ea_0 and 2.03 to 1.39 ea^2_0 , respectively). These results indicate charge donation from the molecule to the $\text{Co}_3\text{Mo}_{13}\text{S}_{32}$ edge and interaction between π electrons of thiophene and the same edge, with some charge transfer to the molecule (backdonation). The picture is further supported by analysis of surface Co atoms: charge and quadrupole values of the $\text{Co}_{\text{e,IV}}^*$ atom, bounded to the S atom of thiophene increase and the quadrupole value of $\text{Co}_{\text{c,IV}}^*$, bonded to the C4 atom of thiophene, also increases due to the electron donation from the molecule to the surface. Similarly to adsorption on the Ni surface, the results indicate C=C bond weakening.

Increase of C=C dipole value in both thiophene adsorption processes indicates a localized induced polarization, thus reflecting a weakening of these bonds, in agreement with increased bond stretches seen in the vibrational analysis, to be discussed.

To summarize, the results for thiophene adsorbed on promoted clusters indicate some interaction between the thiophene π electrons and the surfaces, though not as strong as in bare MoS_2 .³³ Some charge donation from the thiophene molecule to the promoted surfaces is also present. In both cases, the adsorption mode is weaker chemisorption than on bare MoS_2 , an indication of the lower probability of a direct HDS process.

Adsorption energies and harmonic frequencies

Adsorption energies were computed by subtracting the optimized gas-phase thiophene and cluster energies from the energy of the optimized thiophene/cluster complex according to:

$$E_{\text{ad}} = E_{\text{thiophene/cluster}} - E_{\text{thiophene}} - E_{\text{cluster}} \quad (1)$$

For the $\text{Ni}_3\text{Mo}_{13}\text{S}_{32}$ cluster, the computed adsorption energy is 13.7 kcal mol⁻¹, including zero-point-energy corrections. This value is in agreement with a periodic DFT calculation²⁸ yielding 11.5 kcal mol⁻¹; a similar orientation of the adsorbed thiophene molecule on the metal edge was

Table 3. Vibrational frequencies (cm^{-1}) for the isolated thiophene and thiophene adsorbed on the $\text{Ni}_3\text{Mo}_{13}\text{S}_{32}$ and $\text{Co}_3\text{Mo}_{13}\text{S}_{32}$ clusters. The second set of numbers in parenthesis in the NiMoS- and CoMoS-adsorption columns are the shifts with respect to calculated frequencies of the free molecule

Assignment	Experimental (free molecule)	Calculated		
		Free molecule	η^2 -C adsorption (NiMoS)	η^2 -C and η^1 -S adsorption (CoMoS)
$\nu(\text{C-H})$	3126	3284	3276 (-4)	3280 (-8)
$\nu(\text{C-H})$	3125	3282	3271 (-11)	3271 (-11)
$\nu(\text{C-H})$	3098	3231	3241 (+10)	3241 (+10)
$\nu(\text{C-H})$	3098	3219	3229 (+10)	3229 (+10)
$\nu(\text{C=C})$ asym	1507	1594	1554 (-40)	1530 (-64)
$\nu(\text{C=C})$ sym	1409	1491	1441 (-50)	1423 (-68)
$\nu(\text{ring})$	1360	1399	1392 (-7)	1390 (-9)
$\delta(\text{C-H})$	1256	1276	1277 (+1)	1277 (+1)
$\delta(\text{C-H})$	1085	1120	1118 (-2)	1118 (-2)
$\delta(\text{C-H})$	1083	1115	1104 (-11)	1104 (-11)
$\nu(\text{ring})$	1036	1051	1044 (-7)	1048(-3)

also obtained. DFT calculations by Orita *et al.*⁵ using a $\text{Ni}_1\text{Mo}_{15}\text{S}_{32}$ cluster with the metallic edge having two Mo atoms on the corners and only a central Ni atom show that, for thiophene adsorbed vertically, the computed adsorption energy is $7.8 \text{ kcal mol}^{-1}$. Therefore, similarly to thiophene adsorption on bare MoS_2 ,^{15,16,33,40} the most favorable modes for a fully promoted metal edge are parallel to the metallic edge.

The calculated adsorption energy of thiophene molecule adsorbed on the $\text{Co}_3\text{Mo}_{13}\text{S}_{32}$ cluster is $37.1 \text{ kcal mol}^{-1}$, including zero-point-energy corrections. Therefore, this process is more exothermic than adsorption on $\text{Ni}_3\text{Mo}_{13}\text{S}_{32}$. It was not possible to find previous results for thiophene adsorbed on promoted Co catalysts to compare.

Harmonic vibrational frequencies are shown in Table 3. Unscaled gas-phase thiophene vibrational frequencies were computed with the same Gaussian basis set used in this work, including the same pseudo-potentials, to allow consistent comparison with adsorbed thiophene. The comparison of the vibrational frequencies of adsorbed and gas-phase thiophene shows the most important changes occurring in the C=C stretching modes: shifts with respect to calculated frequencies of the free molecule are -50 and -40 cm^{-1} for the symmetric and asymmetric modes in NiMoS adsorption and -64 and -8 cm^{-1} for the symmetric and asymmetric modes in CoMoS adsorption, respectively. This decrease of the stretching frequencies of adsorbed thiophene may be related to participation of thiophene π electrons in the bonds formed between thiophene carbon atoms and the metal surface atoms, as identified according to the partition analysis of the charge density described before.

The frequency shifts of thiophene adsorbed on the promoted systems are substantially smaller than for thiophene adsorbed on bare MoS_2 .^{16,33} This finding provides a further confirmation of the weaker activation of adsorbed thiophene on metal edges of NiMoS and CoMoS catalysts when compared to adsorption on the same edge of bare MoS_2 .

Conclusions

The adsorption of thiophene on clean metal edges of promoted MoS_2 catalysts, described by $\text{Ni}_3\text{Mo}_{13}\text{S}_{32}$ and $\text{Co}_3\text{Mo}_{13}\text{S}_{32}$ clusters, was investigated using DFT. A η^2 coordination type of thiophene adsorbed on the $\text{Ni}_3\text{Mo}_{13}\text{S}_{32}$ cluster and a η^2 -C and η^1 -S mode for adsorption on the $\text{Co}_3\text{Mo}_{13}\text{S}_{32}$ cluster was found after geometry optimization with full relaxation of the coordinates. Computed adsorption energies and final geometries, including zero-point-energy corrections, indicate a weak chemisorption of thiophene molecule on the metallic edge of the $\text{Ni}_3\text{Mo}_{13}\text{S}_{32}$ cluster and a regular chemisorption on the $\text{Co}_3\text{Mo}_{13}\text{S}_{32}$ cluster. Vibrational frequencies and intensities were calculated, and the most important shifts were found for thiophene C=C bonds. Both shifts are lower than for thiophene adsorbed on bare MoS_2 .

From a Coulombic model of bonding strengths using the computed DMA charges, it was possible to show that metal-sulfur bond strengths in the metal edge of promoted catalysts are lower than in bare MoS_2 , thereby confirming the origin of promoter effect as a weakening of surface metal-S bonds.

Geometric, vibrational and electronic results of this work provided a consistent picture of thiophene adsorption

on Ni- and CoMoS₂-promoted catalysts. Moreover, our approach using the distributed multipole analysis offers the possibility for detailed scrutiny of charge density modifications in molecular processes.

Supplementary Information

Tables S1-S6 of computed multipole values of the studied molecular systems are available free of charge at <http://jbcbs.sbq.org.br> as PDF file.

Acknowledgements

The authors thank Conselho Nacional de Desenvolvimento Científico e Tecnológico (CNPq), Fundação de Amparo à Pesquisa do Estado do Rio de Janeiro (FAPERJ) and the Brazilian Army for financial support of this research. A. M. S. thanks Fundação Ricardo Franco, supporter of IME, for a Post-Doc scholarship. We also thank Prof. M. A. C. Nascimento for availability of the JAGUAR program.

References

- Prins, R.; Debeer, V. H. J.; Somorjai, G. A.; *Catal. Rev.: Sci. Eng.* **1989**, *31*, 1.
- Startsev, A. N.; *Catal. Rev.: Sci. Eng.* **1995**, *37*, 353.
- Oyama, S. T.; Gott, T.; Zhao, H. Y.; Lee, Y. K.; *Catal. Today* **2009**, *143*, 94.
- Chianelli, R. R.; Pecoraro, T. A.; Halbert, T. R.; Pan, W. H.; Stiefel, E. I.; *J. Catal.* **1984**, *86*, 226.
- Orita, H.; Uchida, K.; Itoh, N.; *Appl. Catal., A* **2004**, *258*, 115.
- Kogan, V. M.; Nikulshin, P. A.; *Catal. Today* **2010**, *149*, 224.
- Sun, M. Y.; Adjaye, J.; Nelson, A. E.; *Appl. Catal., A* **2004**, *263*, 131.
- Bollinger, M. V.; Jacobsen, K. W.; Nørskov, J. K.; *Phys. Rev. B: Condens. Matter Mater. Phys.* **2003**, *67*, 085410.
- Tenne, R.; Remskar, M.; Enyashin, A.; Seifert, G. In *Carbon Nanotubes – Topics in Applied Physics 111*; Jorio, A.; Dresselhaus, G.; Dresselhaus, M. S., eds.; Springer-Verlag Berlin: Berlin, Germany, 2008, p. 631.
- Diez, R. P.; Jubert, A. H.; *J. Mol. Catal.* **1992**, *73*, 65.
- Gainza, A. E.; Rodriguezarias, E. N.; Ruetter, F.; *J. Mol. Catal.* **1993**, *85*, 345.
- Chen, R.; Xin, Q.; Wang, C. D.; *J. Mol. Catal.* **1994**, *89*, 345.
- Teraishi, K.; *J. Mol. Catal. A: Chem.* **1997**, *126*, 73.
- Yao, X. Q.; Li, Y. W.; Jiao, H. J.; *J. Mol. Struct. THEOCHEM* **2005**, *726*, 81.
- Raybaud, P.; Hafner, J.; Kresse, G.; Toulhoat, H.; *Phys. Rev. Lett.* **1998**, *80*, 1481.
- Cristol, S.; Paul, J. F.; Schovsbo, C.; Veilly, E.; Payen, E.; *J. Catal.* **2006**, *239*, 145.
- Byskov, L. S.; Nørskov, J. K.; Clausen, B. S.; Topsoe, H.; *J. Catal.* **1999**, *187*, 109.
- Raybaud, P.; Hafner, J.; Kresse, G.; Kasztelan, S.; Toulhoat, H.; *J. Catal.* **2000**, *190*, 128.
- Travert, A.; Nakamura, H.; van Santen, R. A.; Cristol, S.; Paul, J. F.; Payen, E.; *J. Am. Chem. Soc.* **2002**, *124*, 7084.
- Sun, M. Y.; Nelson, A. E.; Adjaye, J.; *J. Catal.* **2004**, *226*, 32.
- Chen, Y. Y.; Dong, M.; Wang, J. G.; Jiao, H. J.; *J. Phys. Chem. C* **2010**, *114*, 16669.
- Krebs, E.; Silvi, B.; Raybaud, P.; *J. Chem. Theory Comput.* **2009**, *5*, 580.
- Raybaud, P.; *Appl. Catal. A Gen.* **2007**, *322*, 76.
- Paul, J. F.; Cristol, S.; Payen, E.; *Catal. Today* **2008**, *130*, 139.
- Lauritsen, J. V.; Helveg, S.; Laegsgaard, E.; Stensgaard, I.; Clausen, B. S.; Topsoe, H.; Besenbacher, E.; *J. Catal.* **2001**, *197*, 1.
- Kibsgaard, J.; Tuxen, A.; Knudsen, K. G.; Brorson, M.; Topsoe, H.; Laegsgaard, E.; Lauritsen, J. V.; Besenbacher, F.; *J. Catal.* **2010**, *272*, 195.
- Krebs, E.; Daudin, A.; Raybaud, P.; *Oil Gas Sci. Technol.* **2009**, *64*, 707.
- Sun, M. Y.; Nelson, A. E.; Adjaye, J.; *Catal. Lett.* **2006**, *109*, 133.
- Weber, T.; van Veen, J. A. R.; *Catal. Today* **2008**, *130*, 170.
- Joshi, Y. V.; Ghosh, P.; Venkataraman, P. S.; Delgass, W. N.; Thomson, K. T.; *J. Phys. Chem. C* **2009**, *113*, 9698.
- Aray, Y.; Rodriguez, J.; *J. Mol. Catal. A: Chem.* **2007**, *265*, 32.
- Aray, Y.; Rodriguez, J.; Vidal, A. B.; Coll, S.; *J. Mol. Catal. A: Chem.* **2007**, *271*, 105.
- Borges, I.; Silva, A. M.; Aguiar, A. P.; Borges, L. E. P.; Santos, J. C. A.; Dias, M. H. C.; *J. Mol. Struct. THEOCHEM* **2007**, *822*, 80.
- Silva, A. M.; Borges, I.; *J. Comput. Chem.* **2011**, *32*, 2186.
- Lee, C. T.; Yang, W. T.; Parr, R. G.; *Phys. Rev. B: Condens. Matter Mater. Phys.* **1988**, *37*, 785.
- Hay, P. J.; Wadt, W. R.; *J. Chem. Phys.* **1985**, *82*, 299.
- Frisch, M. J.; Trucks, G. W.; Schlegel, H. B.; Scuseria, G. E.; Robb, M. A.; Cheeseman, J. R.; Montgomery, J. A.; Vreven, T.; Kudin, K. N.; Burant, J. C.; Millam, J. M.; Iyengar, S. S.; Tomasi, J.; Barone, V.; Mennucci, B.; Cossi, B.; Scalmani, G.; Rega, N.; Petersson, G. A.; Nakatsuji, H.; Hada, M.; Ehara, M.; Toyota, K.; Fukuda, R.; Hasegawa, J.; Ishida, M.; Nakajima, T.; Honda, Y.; Kitao, O.; Nakai, H.; Klene, M.; Li, X.; Knox, J. E.; Hratchian, H. P.; Cross, J. B.; Adamo, C.; Jaramillo, J.; Gomperts, R.; Stratmann, R. E.; Yazyev, O.; Austin, A. J.; Cammi, R.; Pomelli, C.; Ochterski, J. W.; Ayala, P. Y.; Morokuma, K.; Voth, G. A.; Salvador, P.; Dannenberg, J. J.; Zakrzewski, J.; Dapprich, S.; Daniels, A. D.; Strain, M. C.; Farkas, O.; Malick, D. K.; Rabuck, A. D.; Raghavachari, K.; Foresman, J. B.; Ortiz, J. V.; Cui, Q.; Baboul, A. G.; Clifford, S.; Cioslowski, J.; Stefanov, B. B.; Liu, G.; Liashenko, A.; Piskorz, P.; Komaromi, I.; Martin, R. L.; Fox, D. J.;

- Keith, T. J.; Al-Laham, M. A.; Peng, C. Y.; Nanayakkara, A.; Challacombe, M.; Gill, P. M. W.; Johnson, B.; Chen, W.; Wong, M. W.; Gonzalez, C.; Pople, J. A.; Gaussian 03, Revision C.02 ed.; Gaussian, Inc.: Pittsburgh, PA, USA, 2003.
38. Jaguar, version 7.9, Schrödinger, LLC, New York, NY, 2012.
39. Pereira, M. S.; da Silva, A. M.; Nascimento, M. A. C.; *J. Phys. Chem. C* **2011**, *115*, 10104.
40. Orita, H.; Uchida, K.; Itoh, N.; *J. Mol. Catal. A: Chem.* **2003**, *193*, 197.
41. Stone, A. J.; *J. Chem. Theory Comput.* **2005**, *1*, 1128.
42. Cramer, C. J.; *Essentials of Computational Chemistry: Theories and Models*; John Wiley & Sons: Chichester, UK, 2004.
43. Borges, I.; *Int. J. Quantum Chem.* **2008**, *108*, 2615.
44. Anders, G.; Borges, I.; *J. Phys. Chem. A* **2011**, *115*, 9055.
45. Rico, J. F.; Lopez, R.; Ema, I.; Ramirez, G.; *J. Mol. Struct. THEOCHEM* **2005**, *727*, 115.
46. Lopez, R.; Rico, J. F.; Ramirez, G.; Ema, I.; Zorrilla, D.; *Comput. Phys. Commun.* **2009**, *180*, 1654.
47. Moraes, T. F.; Borges, I.; *Int. J. Quantum Chem.* **2011**, *111*, 1444.
48. Stone, A. J.; *Chem. Phys. Lett.* **1981**, *83*, 233.
49. Stone, A. J.; Alderton, M.; *Mol. Phys.* **1985**, *56*, 1047.
50. Stone, A. J.; *The Theory of Intermolecular Forces*, vol. 32; Oxford University Press: Oxford, UK, 1997.
51. Price, S. L.; Stone, A. J.; *Chem. Phys. Lett.* **1983**, *98*, 419.
52. Price, S. L.; *Chem. Phys. Lett.* **1985**, *114*, 359.
53. Price, S. L.; *J. Chem. Soc., Faraday Trans.* **1996**, *92*, 2997.
54. Price, S. L.; *Int. Rev. Phys. Chem.* **2008**, *27*, 541.
55. Ma, X. L.; Schobert, H. H.; *J. Mol. Catal. A: Chem.* **2000**, *160*, 409.
56. Bouwens, S.; Vanveen, J. A. R.; Koningsberger, D. C.; Debeer, V. H. J.; Prins, R.; *J. Phys. Chem.* **1991**, *95*, 123.
57. Leliveld, B. R. G.; van Dillen, J. A. J.; Geus, J. W.; Koningsberger, D. C.; de Boer, M.; *J. Phys. Chem. B* **1997**, *101*, 11160.
58. Sacks, L. J.; *J. Chem. Educ.* **1986**, *63*, 288.
59. Sacks, L. J.; *J. Chem. Educ.* **1986**, *63*, 373.
60. Atkins, P. W.; *Physical Chemistry*; Oxford University Press: Oxford, UK, 1998.
61. Huheey, J. E.; Keiter, E. A.; Keiter, R. L.; *Inorganic Chemistry: Principles of Structure and Reactivity*; Harper Collins College Publishers New York: New York, USA, 1993.
62. Wiegand, B. C.; Friend, C. M.; *Chem. Rev.* **1992**, *92*, 491.

Submitted: April 19, 2012

Published online: September 28, 2012